

Future Change of Western North Pacific Typhoons: Projections by a 20-km-Mesh Global Atmospheric Model*

HIROYUKI MURAKAMI

Japan Agency for Marine-Earth Science and Technology, Meteorological Research Institute, Tsukuba, Ibaraki, Japan

BIN WANG

Department of Meteorology and International Pacific Research Center, University of Hawaii at Manoa, Honolulu, Hawaii

AKIO KITO

Meteorological Research Institute, Tsukuba, Ibaraki, Japan

(Manuscript received 11 March 2010, in final form 24 September 2010)

ABSTRACT

Projected future changes in tropical cyclone (TC) activity over the western North Pacific (WNP) under the Special Report on Emissions Scenarios (SRES) A1B emission scenario were investigated using a 20-km-mesh, very-high-resolution Meteorological Research Institute (MRI)-Japan Meteorological Agency (JMA) atmospheric general circulation model. The present-day (1979–2003) simulation yielded reasonably realistic climatology and interannual variability for TC genesis frequency and tracks.

The future (2075–99) projection indicates (i) a significant reduction (by about 23%) in both TC genesis number and frequency of occurrence primarily during the late part of the year (September–December), (ii) an eastward shift in the positions of the two prevailing northward-recurving TC tracks during the peak TC season (July–October), and (iii) a significant reduction (by 44%) in TC frequency approaching coastal regions of Southeast Asia.

The changes in occurrence frequency are due in part to changes in large-scale steering flows, but they are due mainly to changes in the locations of TC genesis; fewer TCs will form in the western portion of the WNP (west of 145°E), whereas more storms will form in the southeastern quadrant of the WNP (10°–20°N, 145°–160°E). Analysis of the genesis potential index reveals that the reduced TC genesis in the western WNP is due mainly to in situ weakening of large-scale ascent and decreasing midtropospheric relative humidity, which are associated with the enhanced descent of the tropical overturning circulation. The analysis also indicates that enhanced TC genesis in the southeastern WNP is due to increased low-level cyclonic vorticity and reduced vertical wind shear. These changes appear to be critically dependent on the spatial pattern of future sea surface temperature; therefore, it is necessary to conduct ensemble projections with a range of SST spatial patterns to understand the degree and distribution of uncertainty in future projections.

1. Introduction

The first part of this study (Murakami and Wang 2010, hereafter Part I) investigated possible future changes

in tropical cyclone (TC) activity associated with global warming over the North Atlantic (NA), using a 20-km-mesh Meteorological Research Institute (MRI)-Japan Meteorological Agency (JMA) atmospheric general circulation model (AGCM). Here, in Part II of the study, we analyze changes in TC activity over the western North Pacific (WNP) using the same model output.

TC activity in the WNP shows prominent natural variations at various time scales. For example, the Madden-Julian Oscillation (MJO; Madden and Julian 1972, 1994) has a strong influence on TC genesis and occurrence at intraseasonal time scales (Camargo et al. 2009). TC activity also shows interannual and interdecadal variations

* School of Ocean and Earth Science and Technology Publication Number 8031 and International Pacific Research Center Publication Number 727.

Corresponding author address: Hiroyuki Murakami, Meteorological Research Institute (MRI), 1-1, Nagamine, Tsukuba, Ibaraki 305-0052, Japan.
E-mail: hir.murakami@gmail.com

(Chan 1985, 2000; Yumoto and Matsuura 2001; Ho et al. 2004; Wu and Wang 2004), which are strongly affected by various factors associated with low-frequency anomalous climate patterns, such as the El Niño–Southern Oscillation (ENSO; Lander 1994; Chen et al. 1998; Wang and Chan 2002; Wu et al. 2004; Camargo and Sobel 2005), the stratospheric quasi-biennial oscillation (Chan 1995; Ho et al. 2009), and the Pacific decadal oscillation (Wang et al. 2010). Therefore, it is necessary to conduct multi-decadal simulations for projecting future changes in TC climatology.

Recent modeling studies have discussed future changes in TC tracks over the WNP. Given the deficiencies of low-resolution global models in faithfully resolving TCs, Wu and Wang (2004) attempted an indirect method for assessing the possible influence of global climate change on TC tracks. The authors demonstrated that the main characteristics of the current climatology of TC tracks can be derived using a trajectory model and the mean TC motion velocity field, which comprises a large-scale steering flow and beta drift (Wang et al. 1998). Based on this trajectory model and the changes in large-scale steering flows projected by the Geophysical Fluid Dynamics Laboratory (GFDL) global warming experiments [Special Report on Emission Scenarios (SRES) A2 and B2 scenarios], the authors predicted that more TCs will take northward-recurving tracks during the period 2030–59. However, their trajectory model did not take into account future changes in TC genesis locations and possible changes in the magnitude of beta drift.

Previous modeling studies that directly evaluated future changes in WNP TC tracks have yielded diverse results. For example, Bengtsson et al. (2007) used the ECHAM5 global climate model with T213 resolution (about 60-km grid size) forced by the projected future sea surface temperature (SST) of the SRES A1B scenario and projected a decrease in TC track density within the WNP except for its eastern portion. In contrast, using a regional model (horizontal resolution of 0.5°) driven by lateral boundary conditions produced by the National Center for Atmospheric Research (NCAR) Community Climate System Model version 2 (CCSM2) under an extremely strong ($6 \times \text{CO}_2$) forcing, Stowasser et al. (2007) predicted that warming leads to significantly more TCs in the South China Sea but little change in TC occurrence in other areas compared with the present-day (PD) experiment. Yokoi and Takayabu (2009) investigated future changes in TC genesis frequency (TGF) over the WNP using five World Climate Research Programme's Coupled Model Intercomparison Project phase 3 (CMIP3) models with medium resolution (T63–T106). Similar to the results obtained by McDonald et al. (2005), the authors reported that the prevailing genesis region in the

WNP shows a significant southeastward shift, similar to that observed during El Niño years. However, the CMIP3 output by the Program for Climate Model Diagnosis and Intercomparison (PCMDI) database (available online at <http://www-pcmdi.llnl.gov/>) has only daily averages, making it difficult to detect TC tracks, especially in midlatitude regions, which are characterized by rapid TC movement.

The future changes projected by the model studies outlined above seem to be inconsistent with the observed trends in the past 40 yr, during which the global mean air temperature has increased by about 0.5°C. Ho et al. (2004) reported that the frequency of TC occurrence showed a significant decrease in the Philippine Sea during 1980–2001 compared with 1951–79. Wu et al. (2005) compared TC frequency between 1965–83 and 1984–2003 using observed best-track data, revealing that the two prevailing TC tracks in the WNP had shifted significantly westward; hence, the frequency of TC occurrence has increased over subtropical East Asia and strongly decreased over the South China Sea. Changes in TC tracks during the past decade have been attributed to the westward extension of the subtropical high (Zhou et al. 2009). Note that the observed TC-track data are insufficient to evaluate the long-term trend because of the low quality of these data collected before the satellite era (Landsea et al. 2006). Nevertheless, taking into account the results of both numerical and observational studies, the overall pattern of future change in TC tracks over the WNP remains inconclusive.

The present study examines future changes in WNP TC tracks and frequency of occurrence simulated by the 20-km-mesh MRI–JMA AGCM. The results are expected to be more reliable than those of previous studies for the following reasons: the model has the highest spatial resolution reported to date, making it suitable to resolve TCs; and the future projection is based on the 18-model ensemble average of future SST change and covers a 25-yr period that includes interannual variation in SST forcing. More importantly, we focus on the causes of future change in the model projections.

The remainder of this paper is organized as follows. Section 2 provides a brief description of the experimental design and analytical methods. Section 3 assesses the model performance in the present-day simulation against observed best tracks. Section 4 presents the projected future changes in TC genesis number, TC tracks, and TC frequency of occurrence (TCF). In section 5, the causes of future changes in TC tracks and TCF are investigated in terms of changes in steering flows, TC translation vectors, TC genesis locations, and TGF. It was found that the change in TC genesis is a critical factor in understanding the changes in TCF and TC tracks. In

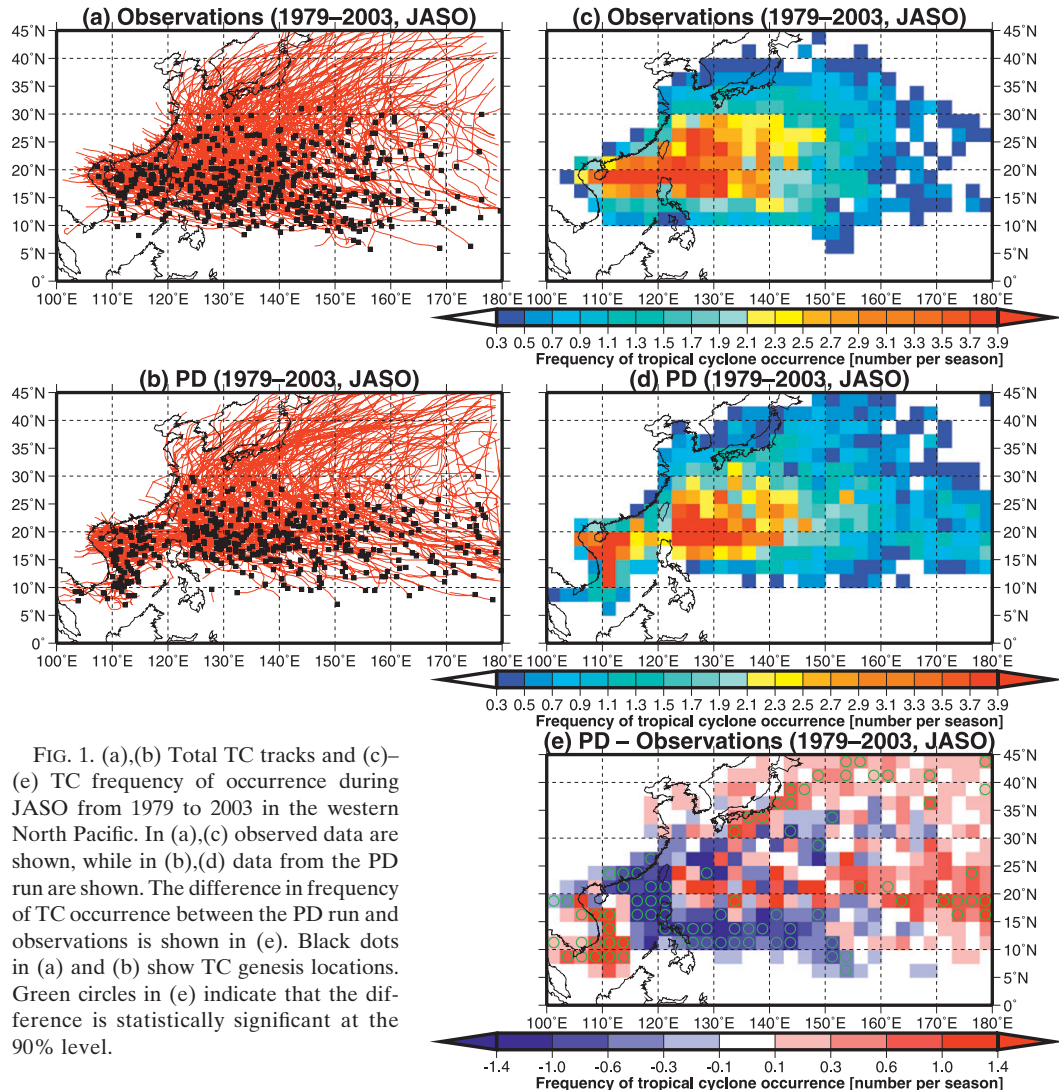


FIG. 1. (a),(b) Total TC tracks and (c)–(e) TC frequency of occurrence during JASO from 1979 to 2003 in the western North Pacific. In (a),(c) observed data are shown, while in (b),(d) data from the PD run are shown. The difference in frequency of TC occurrence between the PD run and observations is shown in (e). Black dots in (a) and (b) show TC genesis locations. Green circles in (e) indicate that the difference is statistically significant at the 90% level.

section 6, the mechanisms responsible for changes in TC genesis locations are further elucidated with reference to the modified genesis potential index (GPI). Finally, a summary of the results is provided in section 7.

2. Methods

a. Model and simulation settings

The climate model, simulation settings, observational data, and strategy for investigating future changes in TC activity, as employed in the present study, are similar to those described in Part I. In short, the AGCM is a hydrostatic and spectral model with a resolution of T959L60 (triangular truncation 959 with a linear Gaussian grid, which is equal to a 20-km mesh horizontally and 60 layers vertically). The model is equipped with a prognostic

Arakawa and Schubert cumulus convection scheme (Randall and Pan 1993), a prognostic cloud scheme (Smith 1990), and the level-2 turbulence closure scheme of Mellor and Yamada (1974) for vertical turbulent diffusion.

The PD realization is a so-called Atmospheric Model Intercomparison Project (AMIP)-style simulation using observed monthly SST and sea ice concentration (SIC) during 1979–2003 [the Hadley Centre Sea Ice and SST dataset version 1 (HadISST1); Rayner et al. (2003)]. For the future global-warmed (GW) simulation, the targeted projection period is the last quarter of the twenty-first century (2075–99). For the lower-boundary conditions in the GW simulation, future changes in SST and SIC were estimated from a CMIP3 multimodel ensemble mean under the SRES A1B scenario to which detrended interannual variations in observed SST were added (Mizuta et al. 2008; Part I), assuming that interannual

variations in SST and SIC in the GW simulation are similar to those of the present day.

b. Detection method for tropical cyclones

The globally uniform TC detection method proposed by Oouchi et al. (2006) results in a marked underestimate of TC genesis number in the WNP (by about 35%) in the PD simulation. To better match the simulated annual number and duration of TCs with observed counterparts in the WNP, a set of modified TC detection criteria was developed for the WNP (see below). To facilitate comparison, the threshold values used in Part I (for the NA) are listed in parentheses.

- 1) Across the 45°S–45°N latitudinal belt, candidate grid points for TC centers are defined as those for which the minimum surface pressure is at least 2.0 hPa lower than the average surface pressure over the surrounding $7^\circ \times 7^\circ$ grid box.
- 2) The magnitude of the maximum relative vorticity at the 850-hPa vertical level exceeds $2.0 \times 10^{-5} \text{ s}^{-1}$ ($3.0 \times 10^{-5} \text{ s}^{-1}$ in Part I).
- 3) The maximum wind speed at the 850-hPa vertical level (WS850) exceeds 10.0 m s^{-1} (14.0 m s^{-1} in Part I).
- 4) The temperature structure aloft has a marked warm core, such that the sum of the temperature deviations at 300, 500, and 700 hPa exceeds 1.0 K (1.2 K in Part I). The temperature deviation for each level is computed by subtracting the maximum temperature from the mean temperature over the surrounding $10^\circ \times 10^\circ$ grid box.
- 5) WS850 is higher than that at 300 hPa (WS300) at the time of first detection. After the first detection, this criterion is no longer applied (in Part I, WS850 plus 2.5 m s^{-1} was required to be greater than WS300 following generation).
- 6) The duration exceeds 36 h.

Note that the threshold values 2), 3), and 4) are lower than those used in Part I. This is necessary because modeled convective activity in the WNP is less intense than that in other basins (Oouchi et al. 2006).

The TC positions were counted for each $2.5^\circ \times 2.5^\circ$ grid over the WNP region (0° – 45°N , 100°E – 180°) at 6-h intervals. The total count for each grid was defined as the TCF. The first detected position was defined as the location of TC genesis, and the TGF at each grid was counted in the same way as that for TCF. Because the computed TGF fields are noisy, we smoothed TGF using 9-point moving average weighted by the distance from the center of the grid. Because TCs in the WNP are generated mainly during the peak season in the boreal summer [July–October (JASO)], this study focuses on TC changes during these months.

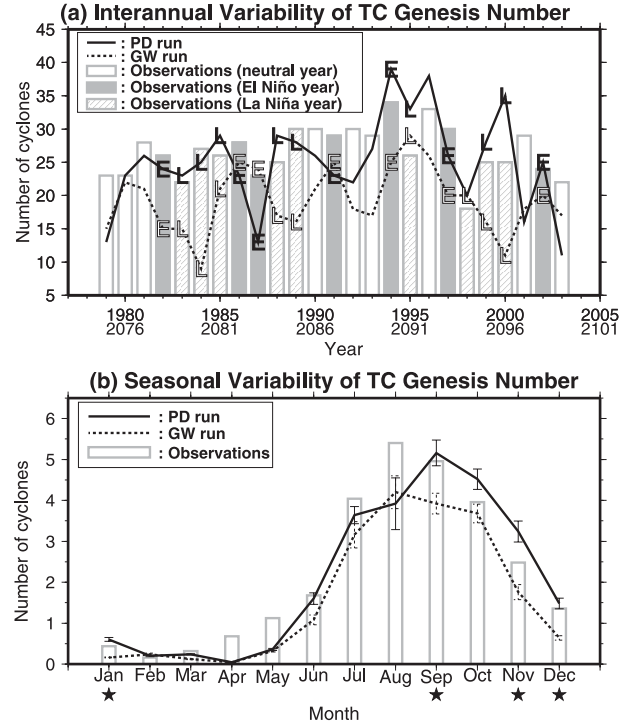


FIG. 2. (a) Yearly and (b) seasonal variability in the number of tropical cyclones, based on observations (1979–2003; histogram), PD run (1979–2003; solid black line), and GW run (2075–99; dotted black line). The correlation coefficient for yearly TC number between the PD run and observations is 0.55, which is statistically significant at the 95% level. The average TC frequencies are 26.6 (observed), 25.0 (PD run), and 19.3 (GW run). The “E” (“L”) in (a) indicates an El Niño (La Niña) year, and stars at the base of (b) indicate a statistically significant difference between the GW and PD runs at the 95% level. The error bars in (b) show the two-sided 95% confidence interval for each GW (dashed) and PD (solid) run.

c. Modified GPI

To determine the factors that influence changes in TC genesis location, we used a modified version of the Emanuel and Nolan (2004) GPI (Part I):

$$\text{GPI}' = |10^5 \eta|^{3/2} \left(\frac{\text{RH}}{50} \right)^3 \left(\frac{V_{\text{pot}}}{70} \right)^3 (1 + 0.1 V_s)^{-2} \left(\frac{-\omega + 0.1}{0.1} \right), \quad (1)$$

where η is the absolute vorticity (s^{-1}) at 850 hPa, RH is the relative humidity (%) at 700 hPa, V_{pot} is the maximum potential intensity (MPI; m s^{-1}) of Emanuel (1995), V_s is the magnitude of the vertical wind shear (m s^{-1}) between 850 and 200 hPa, and ω is the vertical wind velocity (Pa s^{-1}) at the 500-hPa vertical level. The modified version shown in Eq. (1) has a vertical wind velocity term that enables correct reproducibility of TC

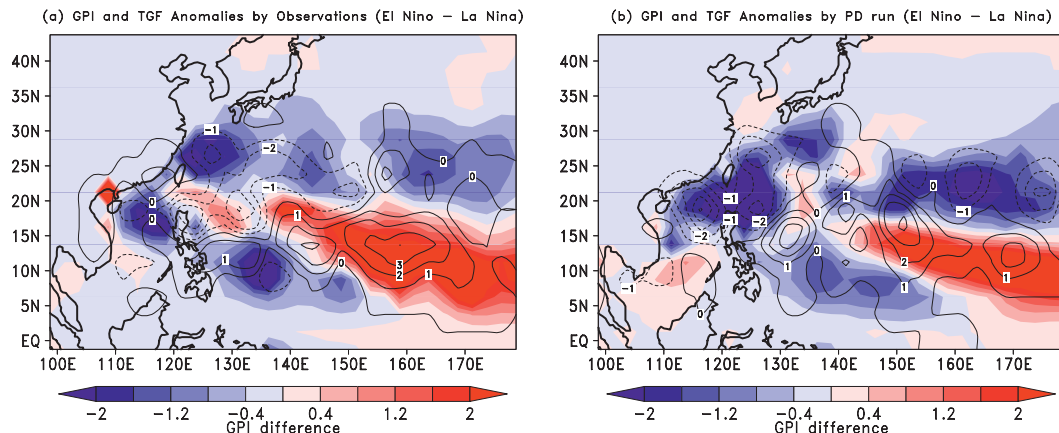


FIG. 3. Mean differences in TGF (contours) and GPI (hatching) between El Niño and La Niña years during the period of JASO obtained from (a) best-track data and (b) the present-day run. Unit is one standard deviation normalized by spatial variation. The observed GPI was computed from the JRA-25 reanalysis dataset (Onogi et al. 2007). El Niño (La Niña) years are defined as 1982, 1986, 1987, 1991, 1994, 1997, and 2002 (1983, 1984, 1985, 1988, 1989, 1995, 1998, 1999, and 2000).

genesis over regions with strong ascending motions, such as the ITCZ. The definition of MPI is based on Emanuel (1995) but as modified by Bister and Emanuel (1998):

$$V_{\text{pot}}^2 = \frac{C_k}{C_D} \frac{T_s}{T_0} (\text{CAPE}^* - \text{CAPE}^b), \quad (2)$$

where C_k is the exchange coefficient for enthalpy, C_D is the drag coefficient, T_s is SST (K), and T_0 is the mean outflow temperature (K). The quantity CAPE^* is the value of convective available potential energy (CAPE) of the air lifted from saturation at sea level, with reference to environmental sounding data, and CAPE^b is that of the boundary layer air. Both quantities are evaluated near the radius of maximum wind, which is iteratively determined assuming the wind field is balanced by the radial pressure gradient in the eye region (a FORTRAN source code for computing the MPI is available online at ftp://texmex.mit.edu/pub/emanuel/TCMAX/pcmin_revised.f).

d. Observational best-track and JRA-25 reanalysis data

The observed TC “best-track” data, obtained from the Web site of the Unisys Corporation (Unisys 2010), was used to evaluate the TC simulation in the PD run. The data were provided by the U.S. Navy’s Joint Typhoon Warning Center (JTWC) for the WNP. In the present study, we only selected TCs with tropical storm intensity or stronger (i.e., those TCs that possess 1-min sustained surface wind of 35 kt or greater). The Japanese 25-yr Reanalysis (JRA-25) Project (JRA-25) dataset

(Onogi et al. 2007) was also used for the GPI analysis to enable a comparison with the model’s GPI.

e. Statistical significance tests

Tests of statistical significance, for evaluating the difference (i.e., increase or decrease) between mean values, were conducted using Welch’s t test, which assumes two samples with possibly unequal variances. This study also considers adjustments of sample sizes (or freedom) by autocorrelations in time series. A standard statistical test depends on the assumption of random samples. However, if a time series of length N is autocorrelated, the number of independent samples (i.e., the effective sample size) is fewer than N . Here, an effective sample size is derived by the following equation (WMO 1966):

$$N' = N \frac{(1 - r_1)}{(1 + r_1)}, \quad (3)$$

where N' is the effective sample size, N is the sample size, and r_1 is the lag-1 (i.e., 1 yr) autocorrelation coefficient. For example, if the sample size is 25 yr and the lag-1 autocorrelation is 0.5, the adjusted sample size is reduced to 8 yr.

3. Evaluation of the present-day simulation

a. TC tracks and frequency of occurrence

The observed and simulated TC tracks and TCF during the peak season of July–October are compared in Fig. 1. Overall, TCF is reasonably well simulated in the PD run (Figs. 1c and 1d), showing a maximum northeast

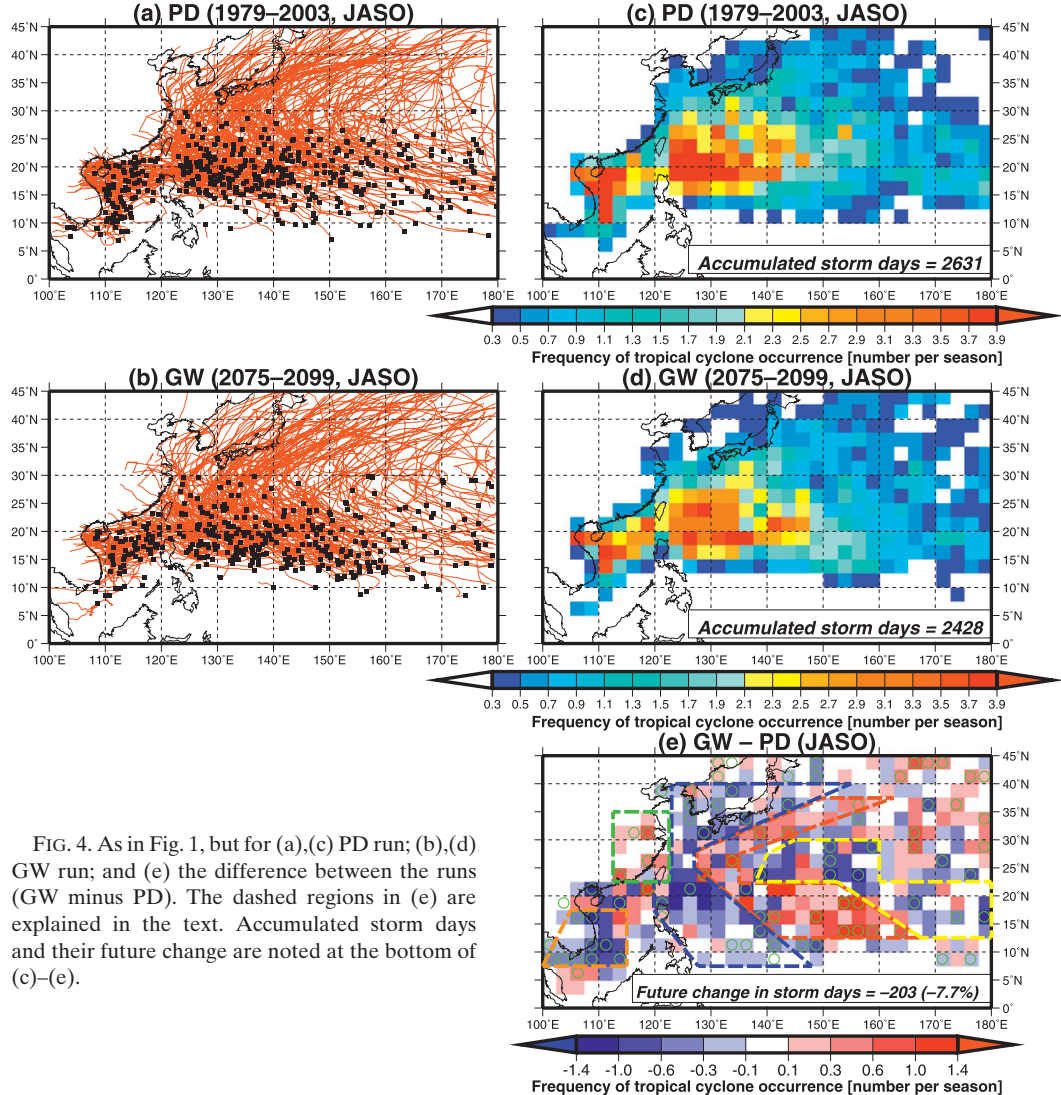


FIG. 4. As in Fig. 1, but for (a), (c) PD run; (b), (d) GW run; and (e) the difference between the runs (GW minus PD). The dashed regions in (e) are explained in the text. Accumulated storm days and their future change are noted at the bottom of (c)–(e).

of the Philippines (20°N , 125°E). However, biases are apparent in Fig. 1e. For example, TCF is severely underestimated in the southern Philippine Sea (10° – 17°N , 122° – 150°E) and in the northeast South China Sea (15° – 25°N , 115° – 122°E), implying that fewer TCs move westward and penetrate into the South China Sea. In addition, TCF is overestimated in the southwest South China Sea (7° – 17°N , 112° – 115°E).

b. Interannual and seasonal variability

Figure 2a compares the observed and simulated total TC genesis numbers counted for each calendar year. The observed and simulated annual (peak season) basin-averaged TC numbers are 26.6 (18.4) and 25.0 (17.2), respectively. Figure 2a shows that some of the local maxima and minima are in good agreement between the PD run (solid black line) and observations (histogram).

The correlation coefficient of interannual variations between the two is 0.55 (0.71) for the annual (peak season) TC number, which is statistically significant at the 99% confidence level (based on the significance test for Pearson's product-moment correlation).

Figure 2b shows seasonal variations in TC genesis number. This annual variation is reasonably well simulated in the PD run, except that the simulated distribution of TC numbers is higher later in the season.

c. Variations in TC genesis influenced by ENSO

ENSO is one of the primary drivers of interannual variations in TCs. Figure 3 shows anomalies of TGF along with the modified GPI anomalies in the peak season for contrasting warm and cold phases of ENSO. Here, we computed the observed JASO mean Niño-3.4 (5°S – 5°N , 120° – 170°W) SST for each year from 1965 to

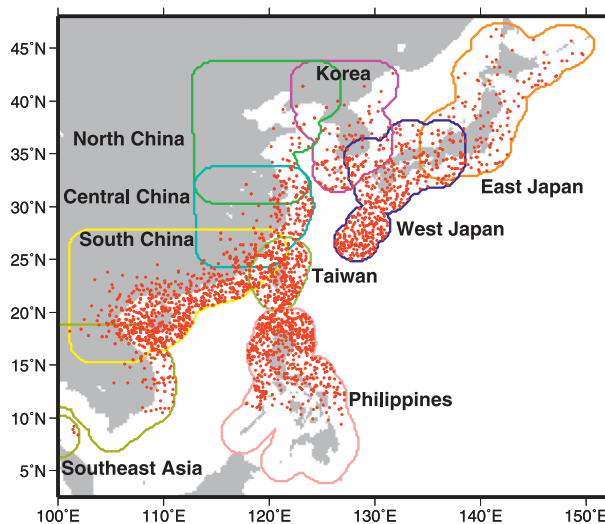


FIG. 5. Observed TCs in the nine coastal regions during JASO of 1979–2003, as derived from 6-hourly data. Red dots show the locations of TCs.

2003. Following Wang and Chan (2002), an El Niño (La Niña) year is defined as a year in which the SST anomaly exceeds (is less than) 0.4 (-0.4) of the standard deviation computed during the period. According to this criterion, El Niño (La Niña) years occurred in 1982, 1986, 1987, 1991, 1994, 1997, and 2002 (1983, 1984, 1985, 1988, 1995, 1998, 1999, and 2000).

The observations (Fig. 3a) reveal a marked southeast–northwest contrast in both TGF and GPI, as respectively reported in Wang and Chan (2002) and Camargo et al. (2007). In the PD run (Fig. 3b), the contrasting features are faithfully reproduced. The spatial correlation between observations and the PD run is 0.67 (0.36) for GPI (TGF), indicating that the variance in TC genesis locations induced by ENSO is reasonably well reproduced. The spatial correlation between the GPI and TGF anomalies is 0.46 (0.47) for observations (the PD

run). Moreover, the correlation coefficient between the annual mean TC number (solid line in Fig. 2a) and the annual mean basin GPI (data not shown) is 0.44, indicating that the modified version of GPI performs reasonably well in capturing interannual variations in TC genesis (the correlation coefficient obtained for the original version of GPI is 0.30). The reasonable agreement obtained between observations and the PD simulation adds confidence to the reliability of the model's future projections.

4. Projected future changes

a. Tropical cyclone genesis number

The dotted lines in Figs. 2a and 2b show interannual and seasonal variability in total TC number in the WNP basin for the GW run, respectively. The annual total number of TCs is 19.3 for the GW run, which represents a reduction of 22.7% compared with the PD run. This difference is statistically significant at the 99% level. Note however, that this reduction occurs only in the late TC season (September–December; Fig. 2b). Recall also that the model simulation of the PD climate is less realistic in the later part of the season. This decrease is in contrast to the result for the NA, as reported in Part I, for which the TC number shows a slight increase in the GW run (although not statistically significant). The interannual variation in TC genesis number in the GW run is slightly different from that in the PD run (the correlation coefficient between the two runs is 0.20, which is not statistically significant), although the two runs share the same interannual variation in SST forcing.

b. Frequency and tracks

Figure 4 compares TC tracks and TCF between the PD and GW runs for the peak season of July–October, revealing marked differences (Fig. 4e), including a region

TABLE 1. Accumulated tropical cyclone storm days in nine coastal regions during the July–October season: observations (1979–2003), PD run (1979–2003), GW run (2075–99), future change, and level of statistical significance of future change (levels less than 90% are not shown). The off-shore edges of the coastal regions are defined as being 200 km from the coast line.

	Obs (1979–2003)	PD (1979–2003)	GW (2075–99)	GW – PD	Level of statistical significance of the future change
East Japan	44.0	65.0	53.8	$-11.3 (-17.3\%)$	—
West Japan	124.0	119.0	95.5	$-23.5 (-19.7\%)$	—
Korea	31.3	34.3	25.8	$-8.5 (-24.8\%)$	—
North China	15.0	18.5	24.8	$+6.3 (+33.8\%)$	—
Central China	53.0	32.5	51.3	$+18.8 (+57.7\%)$	—
South China	194.0	147.3	134.0	$-13.3 (-9.0\%)$	—
Taiwan	70.0	55.5	59.5	$+4.0 (+7.2\%)$	—
Southeast Asia	40.5	94.8	53.5	$-41.3 (-43.5\%)$	99%
Philippines	145.0	66.8	51.3	$-15.5 (-23.2\%)$	—

TABLE 2. As in Table 1, but for the average instantaneous maximum wind velocity (m s^{-1}).

	Obs (1979–2003)	PD (1979–2003)	GW (2075–99)	GW – PD	Level of statistical significance of the future change
East Japan	27.9	20.9	22.4	+1.5 (+7.4%)	95%
West Japan	35.9	23.4	25.1	+1.7 (+7.2%)	95%
Korea	28.0	20.0	20.4	+0.4 (+1.8%)	—
North China	24.8	15.2	15.8	+0.7 (+4.4%)	—
Central China	29.0	17.4	17.6	+0.2 (+1.1%)	—
South China	28.8	16.5	17.8	+1.2 (+7.4%)	99%
Taiwan	35.6	20.1	20.3	+0.2 (+1.0%)	—
Southeast Asia	27.5	16.6	17.5	+1.0 (+5.8%)	90%
Philippines	34.5	17.7	19.2	+1.5 (+8.7%)	95%

of decrease (outlined by the dashed blue line in Fig. 4e) and a region of increase (dashed red line) immediately east of the belt of decrease. This finding indicates that a larger number of northward-recurving TCs would tend to travel along a path farther to the east than they do in the present day, resulting in a decrease in the number of TCs making landfall over or passing close to Korea and Japan. There also exists a region of increased TCF in eastern China (dashed green line) and a region of decreased TCF (dashed orange line) in the South China Sea, although there is a TCF bias that exists in the South China Sea (Fig. 1e). TCF also shows a decrease in the far-eastern WNP (dashed yellow line), which is marked by a positive TCF bias (Fig. 1e).

The basin-scale total frequency of TC occurrence is predicted to decrease in the future for every month except August. The percentage decrease for the peak season (all seasons) is 7.7% (22.6%). The decrease in total frequency is smaller than the 13.2% decrease in the total TC genesis number during the peak season. This finding indicates that the mean TC life span will increase in the future, apparently because more TCs will tend to travel over the warm open ocean of the far-east WNP, thereby reducing their chance of making landfall and enhancing their chance of intensifying (Chan and Liu 2004).

c. TCs approaching land

The evaluation of future change in the frequency of TC landfall is important for estimating storm-related socioeconomic losses in the future. Figure 5 shows observed TCs within the coastal regions of East Asia (within 200 km of the outer edge of the model's land surface grid) for nine subregions (east Japan, west Japan, Korea, north China, central China, south China, Southeast Asia, Taiwan, and the Philippines). Note that overlaps exist among these regions. The same results as those described below were also obtained for storms within 300 km of the outer edge (data not shown). Table 1 lists the statistics regarding projected accumulated storm days (i.e., the TC frequency derived from 6-hourly data divided by four) for periods when TCs are located in the coastal domains during the peak season of July–October. Most coastal regions show reasonable agreement between the PD run and observations, although considerable discrepancies exist in Southeast Asia and the Philippines, consistent with the error map of TCF (Fig. 1e). In terms of future changes, the largest significant reduction (by 44%) is seen over Southeast Asia.

When the instantaneous maximum surface wind velocities for TCs are averaged (Table 2), all coastal regions show an increasing intensity (by 1%–8%), indicating that

TABLE 3. As in Table 1, but for the July–October mean number of landfalling tropical cyclones.

	Obs (1979–2003)	PD (1979–2003)	GW (2075–99)	GW – PD	Level of statistical significance of the future change
East Japan	0.60	0.44	0.44	0.00 (0.0%)	—
West Japan	1.24	0.64	0.60	-0.04 (-6.3%)	—
Korea	0.76	0.32	0.28	-0.04 (-12.5%)	—
North China	0.12	0.12	0.12	0.00 (0.0%)	—
Central China	0.72	0.36	0.44	+0.08 (+22.2%)	—
South China	4.40	1.64	1.68	+0.04 (+2.4%)	—
Taiwan	1.16	0.36	0.48	+0.12 (+33.3%)	—
Southeast Asia	0.52	0.80	0.52	-0.28 (-35.0%)	—
Philippines	1.96	0.40	0.36	-0.04 (-10.0%)	—

TC events become increasingly severe in the future, regardless of any change in TC frequency. Because the model underestimates the intensity compared with observations (Murakami and Sugi 2010), the degree of intensification remains uncertain.

Table 3 lists the future change in mean TC number of landfalls for the peak season, which differs from the frequency of TCs (Table 1). For the future changes, all regions show somewhat similar changes to those in Table 1, except that these changes are statistically insignificant.

5. Reasons for future change in TC frequency

Changes in large-scale flows and TC genesis frequency

The changes in TCF can be explained largely in terms of the TC genesis locations and motions. The latter is in turn affected by changes in large-scale steering flows. Here, we compare the climatological mean TC translation vectors between the PD and GW runs. The mean TC translation vectors are computed at every $2.5^\circ \times 2.5^\circ$ grid point based on all the TCs that passed across each point. July–October mean motion vectors and future change are shown in Fig. 6. Note that more than 15 storms are required to construct a mean motion vector in a grid. The mean vector norm is respectively 3.67 and 3.42 m s^{-1} for the PD run (Fig. 6a) and GW run (Fig. 6b), indicating, on average, a slightly reduced TC motion speed in the future. Moreover, the future change (Fig. 6c) in the mean zonal (meridional) component is respectively $0.36 (-0.06) \text{ m s}^{-1}$ and $0.65 (-0.11) \text{ m s}^{-1}$ for the entire basin and regions south of 20°N , indicating a significant future “slow down” in the westward translation speed. This reduced speed is especially pronounced in tropical regions around 135°E and east of 150°E .

The vectors in Fig. 7 show future changes in simulated mass-weighted, large-scale steering flows between the 850- and 300-hPa vertical levels. Overall, the projected future changes in large-scale steering flows are markedly different from those reported by Wu and Wang (2004), who reported that easterly (westerly) anomalies dominated in the tropics (midlatitudes). In the future projection, the easterly flows are significantly weakened south of 20°N and east of 130°E , which is consistent with the changes in TC translation vectors shown in Fig. 6. The red (blue) contours in Fig. 6 show the departures of seasonal mean geopotential height at 500 hPa from the global mean for the GW (PD) run. The western Pacific subtropical high retreats eastward in the GW run compared with the PD run, causing anomalous cyclonic steering flows over the WNP. Interestingly, the projected westerly changes in steering flows at lower latitudes are

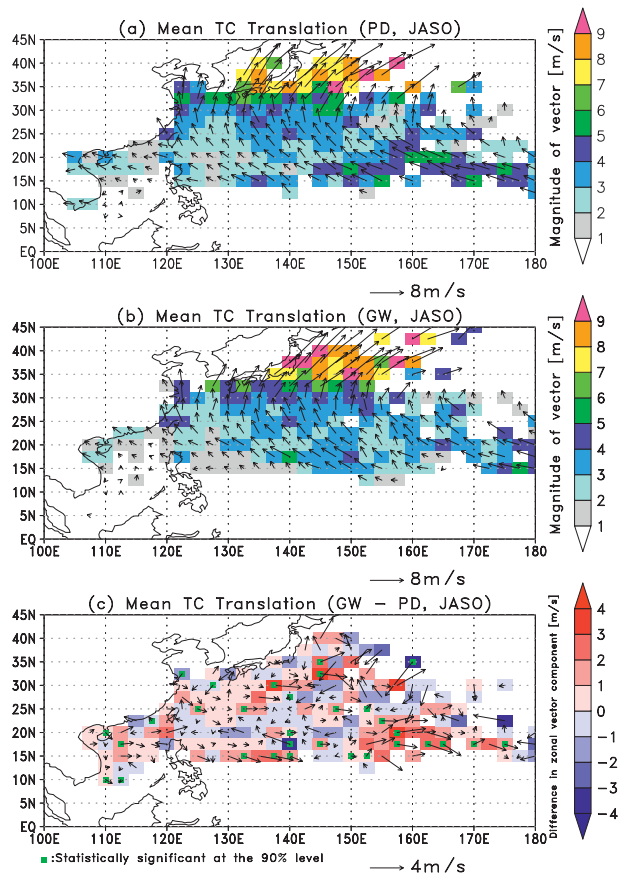


FIG. 6. Simulated mean TC translation vectors and magnitudes (m s^{-1}) for the peak TC season of JASO for (a) the PD run, (b) GW run, and (c) the difference between the GW and PD runs. Data are only shown for grids with more than 15 storms. Green dots in (c) indicate that the vector difference of either the zonal or meridional component is statistically significant at the 90% level. Color shading in (c) indicates differences in the zonal vector component.

similar to observed changes between periods 1951–79 and 1980–2001 (Ho et al. 2004), despite a difference in the shift of the subtropical high. However, an observed period of 50 yr may be too short to distinguish a global warming trend from natural variability.

Figure 8a shows projected future changes in TGF during the peak season. Overall, the spatial distributions of seasonal mean changes in TGF (Fig. 8a) show a strong connection with those in TCF (Fig. 4e), especially over the South China Sea and Philippine Sea, suggesting a close linkage between TGF and TCF.

6. Mechanisms of future changes in TC genesis

Here, we investigate the mechanisms of future changes in TC genesis, based on a modified version of the GPI. Figure 8b shows future changes in GPI. A comparison with future changes in TGF (Fig. 8a) indicates that the

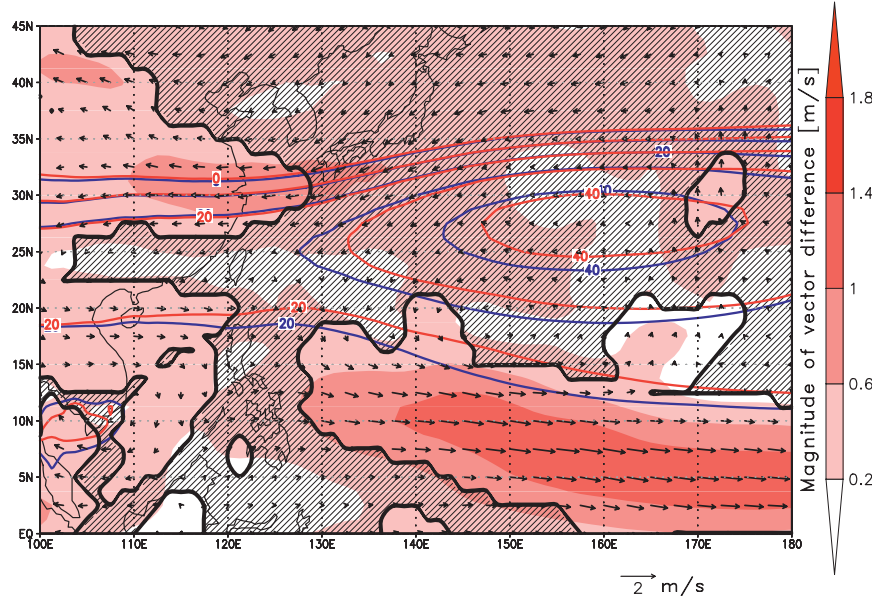


FIG. 7. Simulated future changes in mass-weighted flows (vectors, m s^{-1}) and departures of mean geopotential height at 500 hPa (colored contours, gpm) during the peak season of JASO in the western North Pacific. Black hatching indicates that the vector differences of both the zonal and meridional components are not statistically significant at the 90% level. The departure of geopotential height is computed as the difference from global mean for the PD (blue contours) and GW (red contours) runs. Only positive departures are shown, with an interval of 10 gpm. The global mean of geopotential height is 5852 (5916) gpm for the PD (GW) run.

GPI performs reasonably well in reflecting the changes in TGF (the spatial correlation is 0.55); however, the GPI changes do not perfectly agree with the TGF changes at north of 22.5°N . Although there is room for further improvements in GPI analysis, the GPI can be used to identify those GPI elements that make the greatest contribution to future change.

Figure 9 shows the total future change in the GPI during the peak season of July–October (Fig. 9a), as well as GPI changes obtained by varying each individual GPI element (i.e., variational GPI; Figs. 9b–f). Note that the summation of changes in the variational GPIs is generally equivalent to the total GPI change (Part I).

The MPI (Fig. 9d) is one of the factors causing an increase in GPI for the entire WNP. Here, we investigate which elements in Eq. (2) were responsible for the future increase in MPI and found that among the MPI elements CAPE* was the largest contributor to the increase in MPI (data not shown). CAPE* is determined mainly by SST, indicating that an increase in SST is primarily responsible for the increase in MPI. In general, the effects of relative humidity (Fig. 9c) and MPI (Fig. 9d) tend to cancel each other out, meaning that thermodynamic changes have less influence on TGF changes. Similarly, Chan and Liu (2004) and Chan (2009) reported that because thermodynamical conditions for TC genesis are largely satisfied

in the tropical WNP, dynamical variations are more important in explaining variations in TC genesis. The sign of the GPI contribution is different among the GPI elements; for example, vertical shear and potential intensity act to increase GPI, whereas relative humidity and vertical motion work to decrease it. The reduction in basin-scale TC genesis number seems to reflect a reduction in large-scale ascending motion accompanied by a reduction in relative humidity.

Vecchi and Soden (2007b) reported that in most Intergovernmental Panel on Climate Change (IPCC) Fourth Assessment Report (AR4) models, tropical overturning circulation decreases as the climate warms. Furthermore, the authors noted that the weakening is enhanced in the zonally asymmetric (i.e., Walker) component compared with the zonal mean (i.e., Hadley) component of the tropical circulation. Our projections are consistent with these findings, as we found a weakening in overturning circulation (by 10%–12%) toward the end of the twenty-first century and a more pronounced weakening in the zonally asymmetric component. The decrease in the ascending branch of tropical overturning circulation, accompanied by a decrease in relative humidity, appears to be the main reason for a reduction in total TC formation in the WNP, despite local increases in SST (Sugi and Yoshimura 2004).

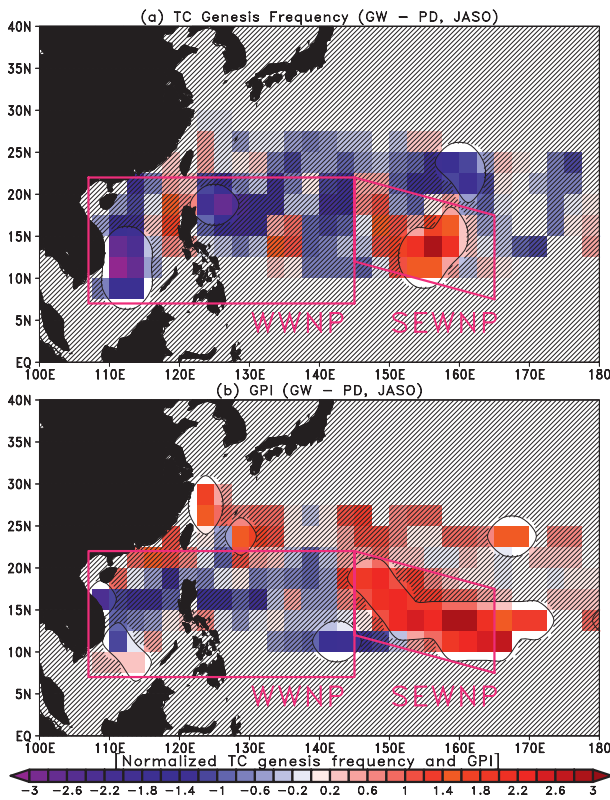


FIG. 8. (a) Future change in the average genesis frequency of tropical cyclones for JASO in the WNP. (b) As in (a), but for future change in GPI. The GPI is filtered out where both present and future climatological mean TGFs are zero. Unit is one standard deviation normalized by spatial variations. Black hatching indicates that the decrease or increase is not statistically significant at the 90% level. Outlined regions are WWNP and SEWNP, which show marked future changes.

For the western WNP (WWNP; as outlined in Fig. 9), the genesis potential shows a marked decrease, due mainly to decreases in vorticity and vertical motions accompanied by reduced relative humidity. In contrast, an increase in genesis potential occurs in southeastern WNP (SEWNP; as outlined in Fig. 9), despite the unfavorable environment for the entire WNP, due to increased low-level vorticity (Fig. 9b) and reduced vertical shear (Fig. 9e).

We examined the causes of these dynamical changes in this region. Figures 10a and 10b show the July–October mean spatial distributions of the streamline at 850 hPa (red lines) and vertical motion at 500 hPa (blue shading), as well as future changes (Fig. 10c). Figure 10d also shows future changes in relative vorticity at 850 hPa (shading) and vertical wind shear (contours) between 850 and 200 hPa. Future changes in vertical motions (Fig. 10c) involve enhanced upward motion north of the equator in the central and eastern Pacific (region E in Fig. 10c).

West of the enhanced upward motion, low-level cross-equatorial flows are intensified in the western Pacific (region F). Moreover, low-level cyclonic vorticity (vertical wind shear) is increased (reduced) in the south-eastern quadrant of the WNP (region G in Fig. 10d). These dynamical changes appear to result from a Rossby wave response induced by equatorially antisymmetric heating (as indicated by upward motion) (Gill 1980); that is, anomalous cyclonic circulation and northward cross-equatorial flows occur west of the heated regions. The Rossby wave response generates anomalous lower-level positive vorticity, extending the monsoon trough eastward. As evidence of this process, the monsoon trough in the WNP in the GW run (C–D in Fig. 10b) extends farther east than that in the PD run (A–B in Fig. 10a). Because the monsoon trough is generally accompanied by weak vertical wind shear (region G in Fig. 10d; Gray 1968; Chia and Ropelewski 2002; Sun and Ding 2002), eastward extension of the trough affects the southeastern quadrant of the WNP basin by providing a favorable dynamical environment for TC generation. In the WWNP, a negative tendency in relative vorticity can also be seen (Fig. 10d). This anomalous negative vorticity may also result from a dynamical response induced by a reduction in diabatic heating in the south-eastern Philippine Sea (region F in Fig. 10c).

The response of heating over the equatorial central Pacific appears to be strongly related to the prescribed future anomaly in SST (Fig. 11a). Over the Pacific, future changes in SST show strong warming in the equatorial central Pacific and subtropical North Pacific, whereas relatively weak warming occurs in the subtropical South Pacific. The resulting thermal contrast between the South and North Pacific results in enhanced cross-equatorial flows in the western Pacific. In addition, the distribution of tropical precipitation changes (Fig. 11b) is strongly correlated with the distribution of tropical SST changes (Fig. 11a). This conclusion has also been reported by Vecchi and Soden (2007a), Sugi et al. (2009), Xie et al. (2010), and Part I, indicating that the spatial distribution of tropical SST changes may be a key factor in determining future changes in TGF.

7. Summary

To evaluate future changes in TC activity over the WNP, we used a 20-km-mesh high-resolution atmospheric general circulation model (MRI–JMA AGCM) to conduct a pair of 25-yr climate simulations for the present day (1979–2003, PD) and for the last quarter of the twenty-first century under a global warming environment (2075–99, GW) based on the SRES A1B scenario.

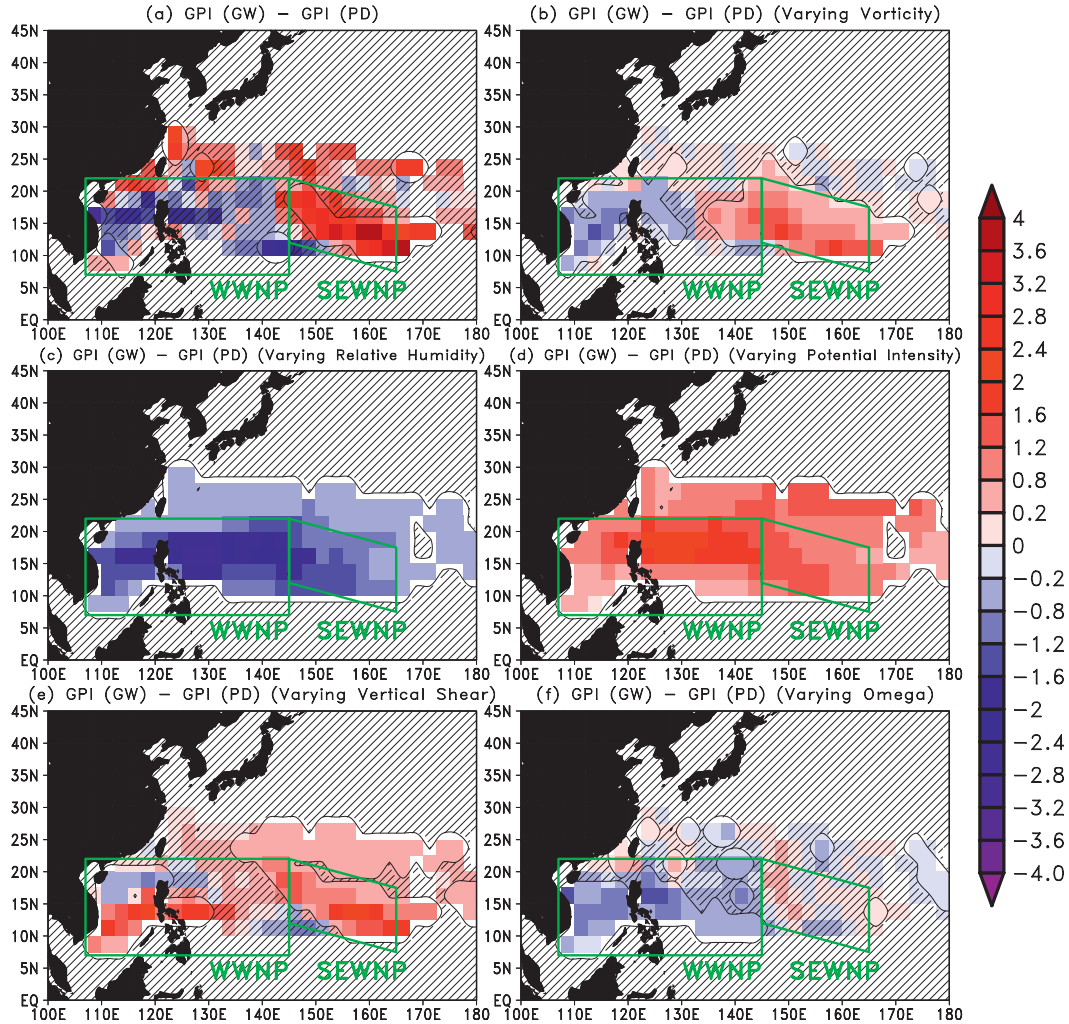


FIG. 9. Future change in the GPI during JASO over the WNP for (a) the difference in GPI between the GW and PD runs, and for GPI changes induced by each individual factor: (b) vorticity, (c) relative humidity, (d) maximum potential intensity, (e) vertical wind shear, and (f) vertical motion. Black hatching indicates that the decrease or increase is not statistically significant at the 90% level. Outlined regions are WNP and SEWNP, which show marked future changes.

The PD simulation demonstrates that the MRI–JMA AGCM performed reasonably well in simulating the climatological mean, seasonal cycle, and interannual variations of TC activity over the WNP. Variations in the spatial distribution of TC genesis between El Niño years and La Niña years were well simulated in the southeastern quadrant of the WNP, revealing an increase (decrease) in GPI and detected TC generation during El Niño (La Niña) years.

Concerning future change, the basinwide TC genesis number (total frequency of occurrence) shows a 13.2% (7.7%) decrease in the GW simulation for the peak season (July–October) and a 22.7% (22.6%) decrease for all seasons (statistically significant at the 95% level). Seasonal variation in TC genesis number showed no

significant future change except for a decrease in autumn and early winter.

Future changes in TCF showed spatial variations. An overall belt of decrease extends from the central WNP (15°N , 140°E) to the east of Taiwan (25°N , 125°E). A belt of substantial increase is seen immediately east of the decreasing belt. These changes indicate that most future TCs will tend to travel along a more eastward course than that of the present day. Consequently, the frequency of TCs is decreased in coastal regions, showing a significant reduction in Southeast Asia (by 44%). Future changes in the number of TC landfalls were not statistically significant.

The cause of changes in TCF was investigated in terms of changes in steering flows and genesis locations. A comparison of steering flows between the PD and GW

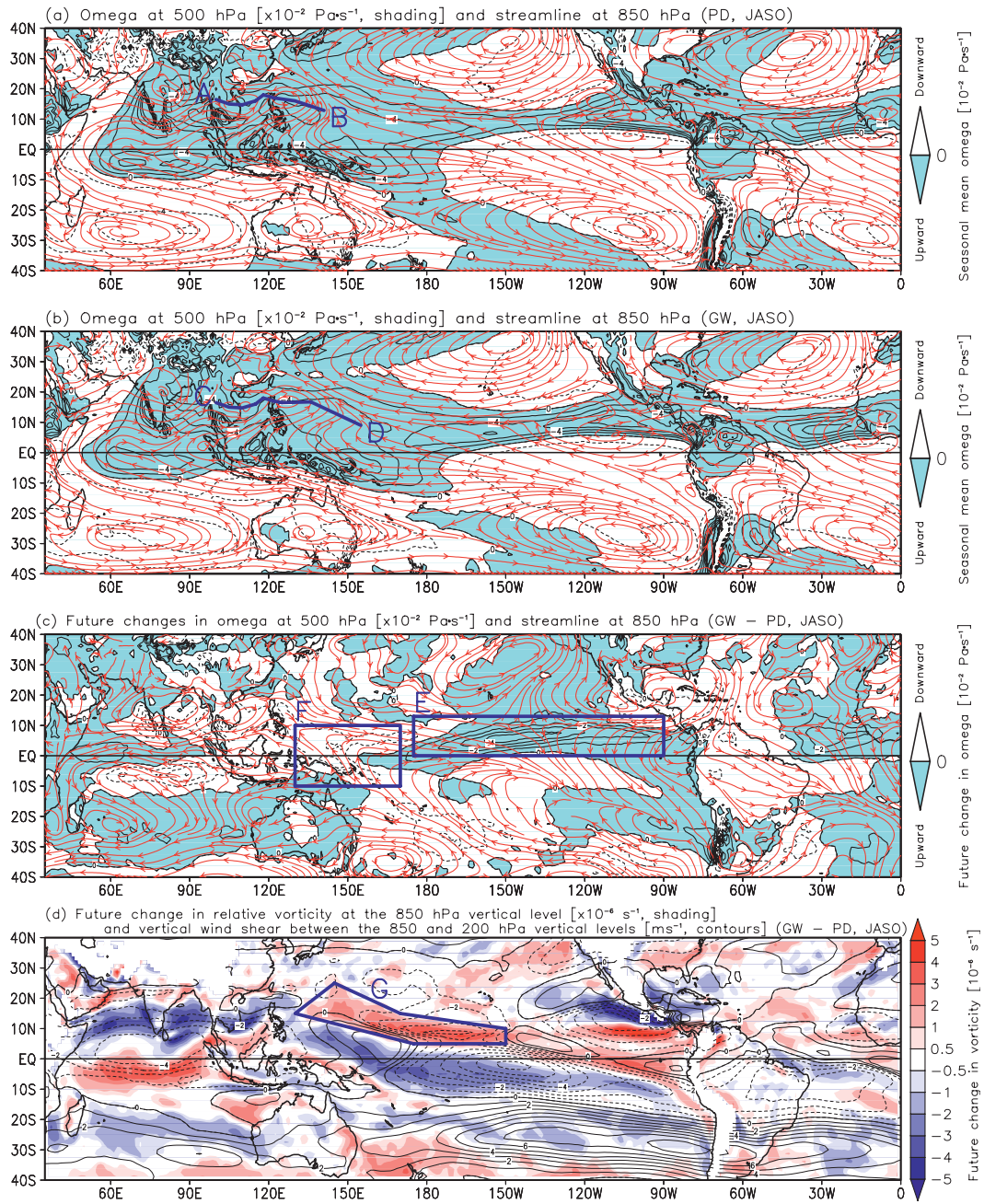


FIG. 10. JASO mean omega (i.e., vertical wind velocity) at 500 hPa (10^{-2} Pa · s $^{-1}$, contours) and streamline at 850 hPa for (a) the PD run, (b) the GW run, and (c) the difference between the GW and PD runs. Dashed contours show positive omega (i.e., descending motion), whereas solid contours with blue shading show negative omega (i.e., ascending motion). (d) Future changes in relative vorticity at 850 hPa (10^{-6} s $^{-1}$, shading) and vertical wind shear between 850 and 200 hPa (m s $^{-1}$, contours). Dashed (solid) contours in (d) indicate reducing (increasing) vertical wind shear. Regions outlined by blue lines with symbols are described in the text.

simulations revealed no significant change north of 20°N, but significant westerly flow anomalies were found in the southeastern quadrant of the WNP, resulting in restriction of the westward motion of TCs. We also found a

marked change in the locations of TC genesis between the PD and GW simulations: TC genesis decreases in the western WNP but increases in the southeastern WNP, consistent with the future change in TCF.

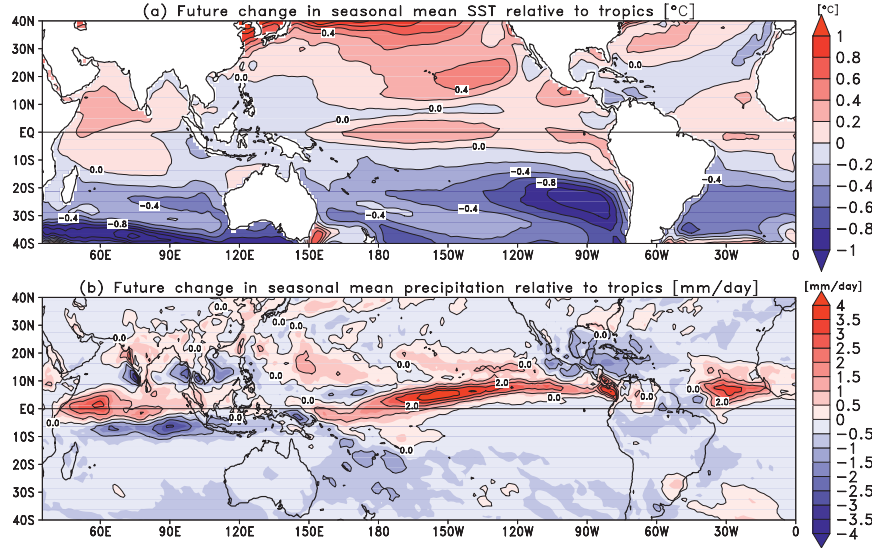


FIG. 11. (a) Future change in seasonal mean prescribed SST ($^{\circ}\text{C}$) relative to the global tropics (20°S – 20°N) for the peak cyclone season of JASO. (b) As in (a), but for precipitation (mm day^{-1}). The tropical mean of SST is 26.9°C (29.0°C) for the present-day (global warming) run, whereas that of precipitation is 4.61 (4.95) mm day^{-1} .

The physical causes of the basinwide decrease in TGF and the change in genesis locations were further elucidated with reference to the modified version of the GPI. The main reasons for the decrease in basinwide and western WNP TGF appeared to be the weakening of the ascending branch of the tropical overturning circulation and reduced tropospheric relative humidity. In turn, these changes are linked to a weakening of the Walker circulation, which is more evident in autumn and early winter. The main factors contributing to the more localized projected future increase in TC genesis in the southeastern WNP are increased lower-level vorticity and reduced vertical wind shear.

The dynamical effects favorable for the increase in TGF in the southeastern WNP appear to have resulted from heating responses in the tropical central Pacific, which act to enhance lower-level vorticity, reduce vertical wind shear, and induce northward cross-equatorial flows. The increased heating over the equatorial central Pacific generally overlaps with the relative SST increase in the future. The enhancement of cross-equatorial flows is also due to interhemispheric contrast in future SST changes. These findings suggest that the mean rising motion tends to decrease throughout the entire WNP in the future global-warmed environment, resulting in a reduced basinwide frequency of TC genesis. However, even under such unfavorable environmental conditions, favorable conditions for TC genesis may arise via the dynamic effects of changes in large-scale flow in the southeastern quadrant of the WNP. Regions of relatively high SST are

important not only in terms of their effect on local TC genesis, but also in their effect on large-scale flows, which in turn has a dynamical effect on the environment of TC genesis and TC motions in the WNP.

Our projections are somewhat different from the observed trend in the past decade and the result of past numerical studies when compared with future changes in large-scale flows and TC tracks. For more reliable future projections, multidecadal ensemble realizations are recommended. The present results suggest that future changes in TC climatology are relatively sensitive to the spatial pattern of relative SST change. This finding indicates that it would be worthwhile to explore the degree of uncertainty in future TC projections by prescribing an SST pattern based on both multimodel ensembles and on results obtained using a range of individual models.

Acknowledgments. This work was conducted under the framework of the “Projection of the Change in Future Weather Extremes Using Super-High-Resolution Atmospheric Models” project supported by the KAKUSHIN program of the Ministry of Education, Culture, Sports, Science, and Technology (MEXT) of Japan. HM would like to thank IPRC for support during his visit to IPRC and thank Professor Yuqing Wang and Tianjun Zhou for useful comments and suggestions. BW acknowledges support from NASA Award NNX09AG97G. Calculations were performed on the Earth Simulator.

REFERENCES

- Bengtsson, L., K. I. Hodges, M. Esch, N. Keenlyside, L. Kornblueh, J.-J. Luo, and T. Yamagata, 2007: How may tropical cyclones change in a warmer climate? *Tellus*, **59A**, 539–561.
- Bister, M., and K. A. Emanuel, 1998: Dissipative heating and hurricane intensity. *Meteor. Atmos. Phys.*, **52**, 233–240.
- Camargo, S. J., and A. H. Sobel, 2005: Western North Pacific tropical cyclone intensity and ENSO. *J. Climate*, **18**, 2996–3006.
- , K. A. Emanuel, and A. H. Sobel, 2007: Use of a genesis potential index to diagnose ENSO effects on tropical cyclone genesis. *J. Climate*, **20**, 4819–4834.
- , M. C. Wheeler, and A. H. Sobel, 2009: Diagnosis of the MJO modulation of tropical cyclogenesis using an empirical index. *J. Atmos. Sci.*, **66**, 3061–3074.
- Chan, J. C. L., 1985: Tropical cyclone activity in the northwest Pacific in relation to the El Niño–Southern Oscillation phenomenon. *Mon. Wea. Rev.*, **113**, 599–606.
- , 1995: Tropical cyclone activity in the western North Pacific in relation to the stratospheric quasi-biennial oscillation. *Mon. Wea. Rev.*, **123**, 2567–2571.
- , 2000: Tropical cyclone activity over the western North Pacific associated with El Niño and La Niña events. *J. Climate*, **13**, 2960–2972.
- , 2009: Thermodynamic control on the climate of intense tropical cyclones. *Proc. Roy. Soc. London*, **A465**, 3011–3022.
- , and K. S. Liu, 2004: Global warming and western North Pacific typhoon activity from an observational perspective. *J. Climate*, **17**, 4590–4602.
- Chen, T.-C., S. P. Weng, N. Yamazaki, and S. Kiehne, 1998: Interannual variation in the tropical cyclone formation over the western North Pacific. *Mon. Wea. Rev.*, **126**, 1080–1090.
- Chia, H. H., and C. F. Ropelewski, 2002: The interannual variability in the genesis location of tropical cyclones in the Northwest Pacific. *J. Climate*, **15**, 2934–2944.
- Emanuel, K. A., 1995: Sensitivity of tropical cyclones to surface exchange coefficients and a revised steady-state model incorporating eye dynamics. *J. Atmos. Sci.*, **52**, 3969–3976.
- , and D. S. Nolan, 2004: Tropical cyclone activity and global climate. Preprints, 26th Conf. on Hurricanes and Tropical Meteorology, Miami, FL, Amer. Meteor. Soc., 240–241.
- Gill, A. E., 1980: Some simple solutions for heat-induced tropical circulation. *Quart. J. Roy. Meteor. Soc.*, **106**, 447–462.
- Gray, W. M., 1968: Global view of the origin of tropical disturbances and storms. *Mon. Wea. Rev.*, **96**, 669–700.
- Ho, C.-H., H.-S. Kim, J.-H. Jeong, and S.-W. Son, 2009: Influence of stratospheric quasi-biennial oscillation on tropical cyclone tracks in the western North Pacific. *Geophys. Res. Lett.*, **36**, L06702, doi:10.1029/2009GL037163.
- Ho, C.-J., J.-J. Baik, J.-H. Kim, D.-Y. Gong, and C.-H. Sui, 2004: Interdecadal changes in summertime typhoon tracks. *J. Climate*, **17**, 1767–1776.
- Lander, M. A., 1994: An exploratory analysis of the relationship between tropical storm formation in the western North Pacific and ENSO. *Mon. Wea. Rev.*, **122**, 636–651.
- Landsea, C. W., B. A. Harper, K. Hoarau, and J. A. Knaff, 2006: Can we detect trends in extreme tropical cyclones? *Science*, **313**, 452–454.
- Madden, R. A., and P. R. Julian, 1972: Description of global-scale circulation cells in the tropics with a 40–50-day period. *J. Atmos. Sci.*, **29**, 1109–1123.
- , and —, 1994: Observations of the 40–50-day tropical oscillation—A review. *Mon. Wea. Rev.*, **122**, 814–837.
- McDonald, R. E., D. G. Bleaken, D. R. Cresswell, V. D. Pope, and C. A. Senior, 2005: Tropical storms: Representation and diagnosis in climate models and the impacts of climate change. *Climate Dyn.*, **25**, 19–36.
- Mellor, G. L., and T. Yamada, 1974: A hierarchy of turbulence closure models for planetary boundary layers. *J. Atmos. Sci.*, **31**, 1791–1806.
- Mizuta, R., Y. Adachi, S. Yukimoto, and S. Kusunoki, 2008: Estimation of the future distribution of sea surface temperature and sea ice using the CMIP3 multi-model ensemble mean. MRI Tech. Rep. 56, 28 pp. [Available at http://www.mri-jma.go.jp/Publish/Technical/DATA/VOL_56/56.html.]
- Murakami, H., and M. Sugi, 2010: Effect of model resolution on tropical cyclone climate projections. *SOLA*, **6**, 73–76.
- , and B. Wang, 2010: Future change of North Atlantic tropical cyclone tracks: Projection by a 20-km-mesh global atmospheric model. *J. Climate*, **23**, 2699–2721.
- Onogi, K., and Coauthors, 2007: The JRA-25 Reanalysis. *J. Meteor. Soc. Japan*, **85**, 369–432.
- Oouchi, K., J. Yoshimura, H. Yoshimura, R. Mizuta, S. Kusunoki, and A. Noda, 2006: Tropical cyclone climatology in a global warming climate as simulated in a 20-km-mesh global atmospheric model: Frequency and wind intensity analysis. *J. Meteor. Soc. Japan*, **84**, 259–276.
- Randall, D., and D.-M. Pan, 1993: Implementation of the Arakawa–Schubert cumulus parameterization with a prognostic closure. *The Representation of Cumulus Convection in Numerical Models*, Meteor. Monogr., No. 46, Amer. Meteor. Soc., 137–144.
- Rayner, N. A., D. E. Parker, E. B. Horton, C. K. Folland, L. V. Alexander, and D. P. Rowell, 2003: Global analysis of sea surface temperature, sea ice, and night marine air temperature since the late nineteenth century. *J. Geophys. Res.*, **108**, 4407, doi:10.1029/2002JD002670.
- Smith, R. N. B., 1990: A scheme for predicting layer clouds and their water content in a general circulation model. *Quart. J. Roy. Meteor. Soc.*, **116**, 435–460.
- Stowasser, M., Y. Wang, and K. Hamilton, 2007: Tropical cyclone changes in the western North Pacific in a global warming scenario. *J. Climate*, **20**, 2378–2396.
- Sugi, M., and J. Yoshimura, 2004: A mechanism of tropical precipitation change due to CO₂ increase. *J. Climate*, **17**, 238–243.
- , H. Murakami, and J. Yoshimura, 2009: A reduction in global tropical cyclone frequency due to global warming. *SOLA*, **5**, 164–167.
- Sun, Y., and Y. H. Ding, 2002: Anomalous activities of tropical cyclones over the western North Pacific and related large-scale circulation features during 1998 and 1999. *Acta Meteor. Sin.*, **60**, 527–537.
- Unisys, cited 2010: Unisys weather hurricane tropical data. [Available online at <http://weather.unisys.com/hurricane/>.]
- Vecchi, G. A., and B. J. Soden, 2007a: Effect of remote sea surface temperature change on tropical cyclone potential intensity. *Nature*, **450**, 1066–1070.
- , and —, 2007b: Global warming and the weakening of the tropical circulation. *J. Climate*, **20**, 4316–4340.
- Wang, B., and J. C. L. Chan, 2002: How strong ENSO events affect tropical storm activity over the western North Pacific. *J. Climate*, **15**, 1643–1658.
- , R. Elsberry, Y. Wang, and L. Wu, 1998: Dynamics in tropical cyclone motion: A review. *Chinese J. Atmos. Sci.*, **22**, 535–547.

- , Y. Yang, Q.-H. Ding, H. Murakami, and F. Huang, 2010: Climate control of the global tropical storm days (1965–2008). *Geophys. Res. Lett.*, **37**, L07704, doi:10.1029/2010GL042487.
- WMO, 1966: Climatic change. WMO Tech. Note 79, 80 pp.
- Wu, L., and B. Wang, 2004: Assessing impact of global warming on tropical cyclone tracks. *J. Climate*, **17**, 1686–1698.
- , —, and S. Geng, 2005: Growing typhoon influence on East Asia. *Geophys. Res. Lett.*, **32**, L18703, doi:10.1029/2005GL022937.
- Wu, M. C., W. L. Chang, and W. M. Leung, 2004: Impacts of El Niño–Southern Oscillation events on tropical cyclone land falling activity in the western North Pacific. *J. Climate*, **17**, 1419–1428.
- Xie, S.-P., C. Deser, G. A. Vecchi, J. Ma, H. Teng, and A. T. Wittenberg, 2010: Global warming pattern formation: Sea surface temperature and rainfall. *J. Climate*, **23**, 966–986.
- Yokoi, S., and Y. N. Takayabu, 2009: Multi-model projection of global warming impact on tropical cyclone genesis frequency over the western North Pacific. *J. Meteor. Soc. Japan*, **87**, 525–538.
- Yumoto, M., and T. Matsuura, 2001: Interdecadal variability of tropical cyclone activity in the western North Pacific. *J. Meteor. Soc. Japan*, **79**, 23–35.
- Zhou, T., and Coauthors, 2009: Why the western Pacific subtropical high has extended westward since the late 1970s. *J. Climate*, **22**, 2199–2215.